Switchable omnidirectional acoustic insulation through open window structures with ultrathin metasurfaces

Yong Ge,[1,2] Hong-xiang Sun,[1,3,*] Shou-qi Yuan,[1] and Yun Lai[2,†]

[1]*Research Center of Fluid Machinery Engineering and Technology, Faculty of Science, Jiangsu University, Zhenjiang 212013, China*

[2]*MOE Key Laboratory of Modern Acoustics, National Laboratory of Solid State Microstructures, School of Physics, and Collaborative Innovation Center of Advanced Microstructures, Nanjing University, Nanjing 210093, China*

[3]*State Key Laboratory of Acoustics, Institute of Acoustics, Chinese Academy of Sciences, Beijing 100190, China*

(Received 22 December 2018; published 11 June 2019)

We theoretically propose and experimentally realize two types of open window structures that exhibit an unusual functionality of switchable omnidirectional acoustic insulation in two different ways. Both types of open window structures consist of an array of blades that are attached with ultrathin metasurfaces on both sides. Based on the acoustic manipulation ability of the metasurfaces, omnidirectional acoustic insulation can be realized in the open windows. Interestingly, such an effect is switchable by simply changing the configuration of the blade array. For the first type, omnidirectional acoustic insulation can be switched on or off by adjusting the distance between two adjacent blades. For the second type in which the open window structure is composed of an alternative arrangement of two types of blades, acoustic insulation can be controlled by moving one kind of blade horizontally. The proposed open windows have the advantage of broadband omnidirectional acoustic insulation and convenient switching mechanisms. Our work opens up a new approach for acoustic insulation in open structures, with potential applications in a variety of fields, such as noise control and architectural acoustics.

DOI: 10.1103/PhysRevMaterials.3.065203

I. INTRODUCTION

Acoustic insulation and absorption have attracted great attention from both the physics and engineering communities owing to important practical applications, such as noise control and architectural acoustics. The recently emerging acoustic metamaterials (AMMs) [1–8] and acoustic metasurfaces (AMs) [9–14] with unusual acoustic manipulation ability have opened up a new way to design various acoustic insulation or absorption structures.

The early proposed sound insulation structures, fabricated by plate- or membrane-type AMMs [15–18], can reflect incident sound energy, owing to anomalous dynamic mass induced by the antiresonance of membrane structures. To realize nonreflection sound insulation, absorptive structures consisting of various local resonant units were proposed, such as Helmholtz resonators [19–22], the metalayer of a gas bubble [23], membrane resonators [24–26], Mie resonators [27], coplanar chambers [28,29], labyrinthine metamaterials [30,31], and gradient-index metasurfaces [32], in which sound energy can be absorbed and dissipated. However, these aforementioned structures are usually not open structures, which would also hinder the exchange of many entities at both sides, such as air, water, heat, and light, besides sound.

As an approach to design similar acoustic systems with open structure, the coherent perfect absorber [33–35] was adopted to absorb incident sound energy without blocking other entities by introducing an additional coherent wave with the same amplitude and opposite phase. Beyond that, the AM composed of artificial Mie resonators [36], acoustic metacage structure [37], and acoustic metamaterial silencer based on Fano-like interference [38] were also introduced to design open structures with a sound insulation effect. Furthermore, by attaching ultrathin AMs on both sides of tunnels and window blades, uni- or bidirectional acoustic insulation was realized [39–41]. However, these structures were usually designed with a single function without considering modulation and flexibility. Recently, an open window structure with dual functions of unidirectional and bidirectional insulation for plane acoustic sources was realized [42]. However, the switching between dual functions was obtained by rotating window blades, which would inevitably lead to the reduction of daylighting. Moreover, sound sources are generally in the form of an omnidirectional point source in many important practical scenarios. The design of the open window structures with switchable omnidirectional acoustic insulation (SOAI) is still a technical challenge.

In this work, we propose two types of open window structures to realize the SOAI effect. Both open window structures consist of an array of blades that are attached with ultrathin AMs on both sides. Omnidirectional acoustic insulation arises from the acoustic manipulation ability of the AMs. In the first type, we realize the SOAI effect by adjusting the distance between two adjacent blades. The second type of open window is composed of an alternative arrangement of two types of blades, in which the SOAI effect can be obtained by moving one kind of blade horizontally. Moreover, we analyze the physical mechanisms of the SOAI effect and experimentally demonstrate the transmitted characteristics for the two types of open windows. The experimental results agree well with the simulation results.

*Corresponding author: jsdxshx@ujs.edu.cn

†Corresponding author: laiyun@nju.edu.cn

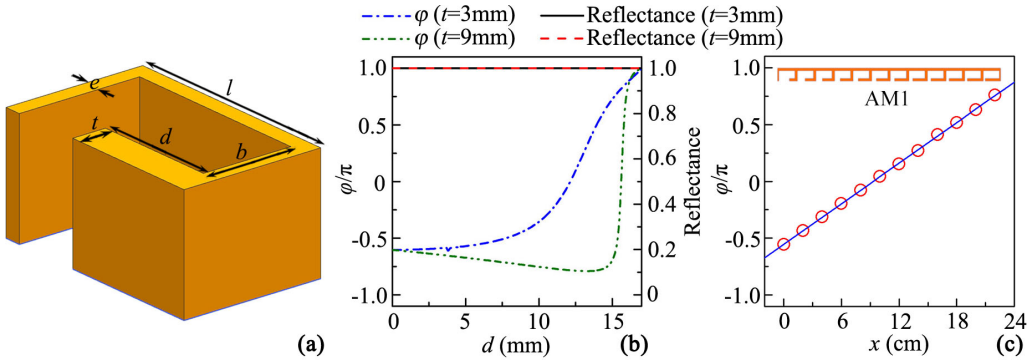

FIG. 1. (a) Schematic of a hooklike meta-atom. (b) Phase delay and reflectance of normally incident wave induced by the hooklike meta-atom as a function of d with $t = 3.0$ and 9.0 mm at 3.5 kHz. (c) Theoretical continuous (blue line) and discrete (red open circles) phase delays of the AM1 (shown in upper inset). The parameter d of 12 selected meta-atoms in the AM1 is 5.8, 9.0, 10.4, 11.2, 11.8, 12.3, 12.7, 13.1, 13.6, 14.0, 14.5, and 15.2 mm from left to right, and $t = 3.0$ mm.

II. BASIC UNIT AND PHASE MANIPULATION

A. Ultrathin hooklike meta-atom

As schematically shown in Fig. 1(a), we propose an ultrathin hooklike meta-atom made of epoxy resin, in which l is the meta-atom length, b is the cavity depth, e is the wall thickness, and t and d are the hook thickness and length, respectively. The proposed meta-atom can reflect the incident acoustic wave and delay its phase heavily. The reflected phase delays can be manipulated by the parameters d and t, and the parameters l and e are 20.0 and 1.5 mm, respectively, and the total thickness $(t + b)$ of the meta-atom remains a constant of 11.0 mm. In this work, we adopt the finite element method (COMSOL MULTIPHYSICS software) to numerically simulate the acoustic propagation characteristics of the designed open windows. The material parameters are listed as follows: the density $\rho = 1180\,\mathrm{kg/m^3}$, the longitudinal wave velocity $c_\mathrm{l} = 2720$ m/s, and the transversal wave velocity $c_\mathrm{t} = 1460$ m/s for epoxy resin; $\rho = 1.21\,\mathrm{kg/m^3}$ and $c_\mathrm{l} = 343$ m/s for air. Figure 1(b) shows the reflected phase delay and the reflectance of the meta-atom with different values of d and t. It is found that the reflectance is almost unity with different parameter d for $t = 3$ and 9 mm. Meanwhile, the reflected phase delay for the normal incident wave can cover almost the whole range of 2π by adjusting the parameters t and d, and therefore we can design an AM with any desired phase distribution based on the result in Fig. 1(b). Figure 1(c) shows the theoretical continuous and discrete phase delays for a designed AM [denoted as AM1, as shown in the upper inset of Fig. 1(c)], in which 12 selected meta-atoms with different parameter d are adopted to realize discrete phase delays of the AM1 with the phase gradient $d\varphi(x)/dx$ of 18.78 rad/m.

B. Acoustic phase manipulation based on AM1

The AM based on the proposed hooklike meta-atoms can realize the manipulation of reflected phase delays for different incident acoustic angles. As shown in Fig. 2(a), in the AM1, the incident or reflected angle is defined as that between the incident or reflected direction and the normal line (red dashed line), and the signs + and − of the incident or reflected angle correspond to the right and left propagation directions, respectively. Thus, the incident angles I1, I2, I3, I4, and I5 [shown in Fig. 2(a)] are 60°, 30°, 0°, −30°, and −60°, respectively. Based on the generalized Snell law [43], the reflected angle θ_r induced by AM is expressed as

$$\theta_\mathrm{r} = \arcsin\left(\sin\theta_\mathrm{i} + \frac{1}{k}\frac{d\varphi(x)}{dx}\right), \tag{1}$$

where θ_i represents the incident angle, and $k = 2\pi/\lambda$ is the wave number in air. Here, according to Eq. (1), the maximum reflected angle is 90°, and its corresponding incident angle is defined as θ_c. So, we rewrite Eq. (1) as $\sin\theta_\mathrm{c} + d\varphi(x)/kdx = 1$, and obtain $\theta_\mathrm{c} = 45°$ for AM1. Based on the critical angle θ_c, the acoustic incidence can be divided into two types. When the incident angle θ_i is larger than θ_c (light blue region), the reflected angle θ_r cannot be obtained based on Eq. (1). As an example, the distribution reflected pressure field induced by AM1 for I1 ($\theta_\mathrm{i} = 60°$) is shown in Fig. 2(b), and a white open arrow represents the reflected direction. Note that the reflected wave propagates to the left side with the reflected angle of −90°, showing that I1 cannot reach the right side of the AM1 and is reflected back directly. So the light blue region is defined as an acoustic blind area (ABA), and the range of the ABA1 is from θ_c to 90°. When the incident angle is smaller than θ_c [yellow region in Fig. 2(a)], the theoretical reflected angles can be obtained by using Eq. (1). Here, we calculate the theoretical reflected angles for the incident waves I2–I5 as 52.5°, 17°, −11.9°, and −35° based on Eq. (1). As shown in Figs. 2(c)–2(f), the simulated reflected angles for I2–I5 agree well with their theoretical results (white open arrows), showing a high performance of phase manipulation for the AM1. Besides, it is necessary to point out that the thickness of the hooklike meta-atoms is only about 0.14λ (λ is the wavelength), and therefore it can be used to design a blade structure for an open window with special functions.

III. RESULTS AND DISCUSSIONS

A. Design of the first type of open window with SOAI effect

Figure 3(a) shows the first type of open window consisting of seven blades attached with AM1 on both sides, in which the parameter w is the distance between two adjacent blades, and LI and RI refer to the left and right incidences of a cylindrical

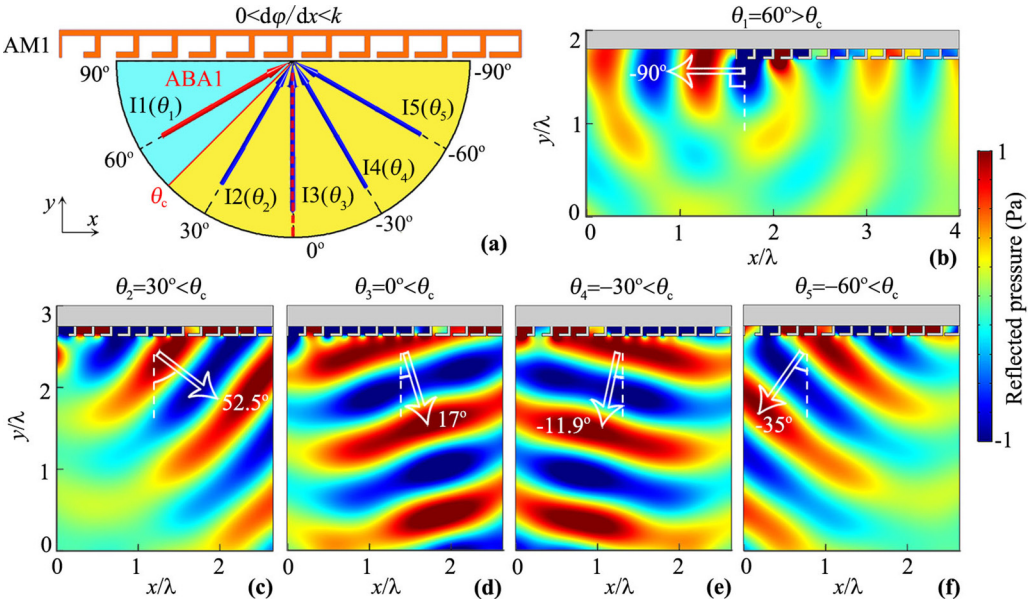

FIG. 2. (a) Schematic of the AM1. The incident angle θ_c corresponds to the maximum reflected angle of 90°. The light blue region is defined as an ABA. The incident acoustic wave I1 is inside the ABA, and the incident acoustic waves I2, I3, I4, and I5 are outside the ABA. Simulated distributions of reflected pressure field induced by the AM1 for the incident acoustic waves (b) I1, (c) I2, (d) I3, (e) I4, and (f) I5 in (a) at 3.5 kHz. White open arrows in (b)–(f) represent theoretical reflected angles.

acoustic source, respectively. Figure 3(b) shows the simulated transmittances of the open window for LI and RI with the distance w from 6.0 to 13.0 cm. In the simulations, the perfectly matched layers are utilized as the outside boundaries of the model, and the cylindrical acoustic source is placed a distance of 2.0 cm away from the open window for both LI and RI cases. The transmittances are obtained by integrating acoustic intensity with and without the open window in the same transmitted region, which is shown in the Supplemental Material [44]. It is found that, in the blue shaded region ($6.0 < w < 9.6$ cm), the transmittances for both LI and RI are below -10 dB, which indicates that the transmitted acoustic energy is very weak. However, when w is larger than 10.3 cm (red shaded region), the transmittances for both LI and RI are larger than -5 dB, showing that the acoustic waves can pass through the open window on both sides.

B. Performance of the first type of open windows

To further show its SOAI characteristic, we simulate the transmittance spectra of the open window with the parameter

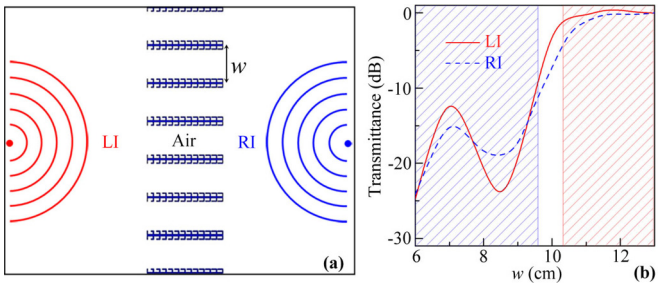

FIG. 3. (a) Schematic of the SOAI open window. (b) Simulated transmittances for LI and RI as a function of w at 3.5 kHz.

$w = 8.0$ and 12.0 cm, which is shown in Figs. 4(a) and 4(b), respectively. For $w = 8.0$ cm [shown in Fig. 4(a)], the transmittance spectra are almost the same for both LI and RI, and keep lower than -10 dB in the range 2.30–4.20 kHz (blue shaded region). Note that the fractional bandwidth (the ratio of the bandwidth to the center frequency) of the omnidirectional acoustic insulation can reach about 0.58. But for $w = 12.0$ cm [Fig. 4(b)], the transmittances are larger than -5 dB in the range 2.95–4.20 kHz for both LI and RI (red shaded region). Therefore, the omnidirectional acoustic insulation of the open window can be switched by adjusting the parameter w.

However, in Fig. 4(b), the transmittances are very low in the range 2.30–2.95 kHz, which arises from a large acoustic wavelength at the low-frequency region. Therefore, by increasing w, the acoustic wave in this range can pass through the open window. To demonstrate it, we simulate the transmittance spectra for $w = 15.0$ cm, which is shown in the Supplemental Material [44]. The result shows that the transmittances for both LI and RI in the range 2.30–2.95 kHz are larger than -7 dB, which demonstrates that the acoustic wave at the low-frequency region can pass through the open window with the larger value of w.

Figures 4(c) and 4(d) show the simulated distributions of the pressure field through the open window with $w = 8.0$ cm for LI and RI, respectively. It is obvious that the cylindrical acoustic waves are insulated by the open window for both cases, and the transmitted acoustic energy is very weak. More importantly, the pressure distributions in each tunnel of the open window for LI and RI are different, indicating different acoustic insulation mechanisms for LI and RI, which is discussed later. Additionally, the omnidirectional acoustic insulation always exists when the cylindrical acoustic sources A and B move along the lines I–IV [Figs. 4(c) and 4(d)], which is shown in the Supplemental Material, Movies I–IV [44],

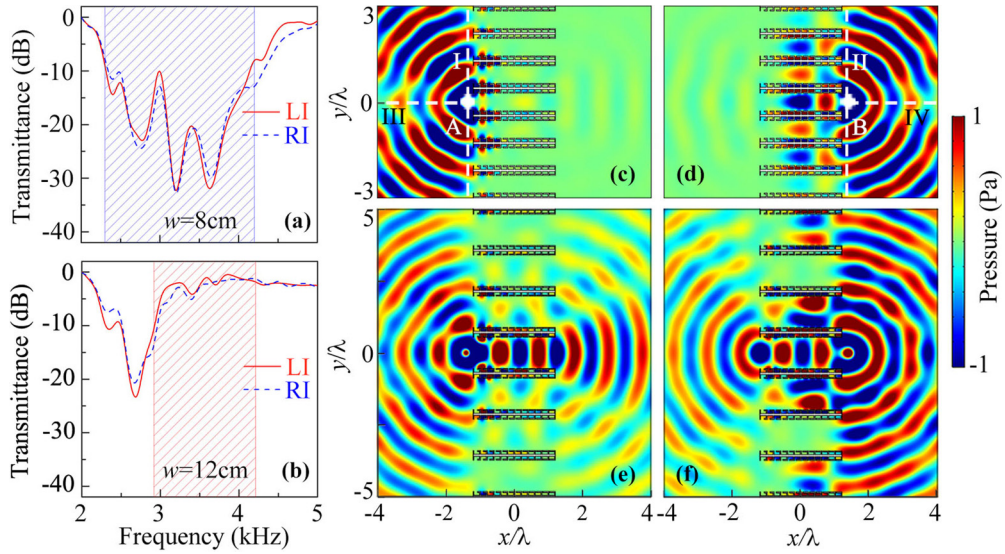

FIG. 4. Simulated transmittance spectra of the open windows with the parameter w of (a) 8.0 cm and (b) 12.0 cm, and simulated distributions of the pressure field induced by the open windows with $w = 8.0$ cm for (c) LI and (d) RI, and with $w = 12.0$ cm for (e) LI and (f) RI at 3.5 kHz. White dots A and B in (c) and (d) represent the position of a cylindrical acoustic source for LI and RI.

respectively. It is further demonstrated that the acoustic insulation for the open window is omnidirectional on both sides. We also discuss the influences of the viscothermal loss on the omnidirectional acoustic insulation of the open window for LI and RI, which is shown in the Appendix. Furthermore, we can switch the omnidirectional acoustic insulation by mechanically adjusting the parameter w. As an example, the transmitted acoustic waves for $w = 12.0$ cm are very obvious for both LI and RI [shown in Figs. 4(e) and 4(f)], which indicates that the open window has high SOAI performance without changing the structure of the AM1. The proposed SOAI window can be applied to insulate noise produced by various machines in machine rooms, such as water pumps and engines, and the heat energy produced by these machines can freely transmit into the external space through the open window. Moreover, the working band of the SOAI window can be reduced around 1.0 kHz by improving the structure of the hooklike meta-atom, which is shown in the Supplemental Material [44].

C. Mechanism of SOAI for the first type of open windows

To gain insight into the mechanism of SOAI, we further discuss acoustic propagation paths in the tunnel of two open windows with the parameters w_1 and w_2 (shown in Fig. 5), respectively. The parameters w_1 and w_2 are selected in the blue and red regions shown in Fig. 3(b). Owing to the omnidirectional incident angles (in the range from $-90°$ to $90°$) of the cylindrical acoustic source, we only consider the incident waves with critical angles for LI and RI to simplify the analysis. As shown in Fig. 5(a), the critical angle of the incident wave I1 (red arrows) for RI is $-90°$. According to Eq. (1), the reflected angle of I1 increases rapidly with the increase of the reflection times between the upper and lower AM1. Therefore, the reflected angle of I1 reaches zero or positive values before I1 passes through the open window with the small value of w. Meanwhile, the other incident wave for RI with the incident angles from $-90°$ to $0°$ cannot transmit through the open window. For LI, the critical angle of the incident wave I2 (blue arrows) is $0°$. In this case, after several reflections between the upper and lower AM1, the reflected angle of I2 is in the range of the ABA1 [from $45°(\theta_{c1})$ to $90°$], and thus I2 is reflected back directly by the AM1. Based on this mechanism, the incident waves for LI with other incident angles also cannot pass through the open window. Therefore, we deduce that the mechanisms of the omnidirectional acoustic insulation for RI and LI are different, which agrees well with the pressure distributions inside the tunnels in Figs. 4(c) and 4(d).

When the parameter w_1 is increased to w_2 [shown in Fig. 5(b)], the propagation distance of each reflection increases gradually, and thus the incident wave I3 for RI can transmit through the window before its reflected angle increases to zero or positive values. Furthermore, the incident wave I4 for LI (blue arrows) can also transmit through the open window before its reflected angle increases to that in the range of ABA1. We deduce that the omnidirectional acoustic insulation of the open window arises from the multiple reflections for RI and the ABA for LI, and the switch of the omnidirectional acoustic insulation is attributed to the increasing propagation distance of each reflection induced by the increase of w.

D. Design of the second type of open windows with SOAI effect

In the first type, the SOAI effect is realized by adjusting the distance w between the adjacent blades. However, in some practical scenarios, the height of the open window is fixed, and the distance w cannot be adjusted. To overcome this challenge, we propose a composite AM consisting of two short metasurfaces (denoted as AM2 and AM3) to design another type of open window by moving the horizontal position of the window blades. Figure 6(a) shows the theoretical continuous phase distribution (blue solid lines) of the composite AM, in which the phase gradients $d\varphi(x)/dx$ of the AM2 ($0 \leqslant x \leqslant 0.1$ m) and AM3 ($0.12 \leqslant x \leqslant 0.22$ m) are 64.11

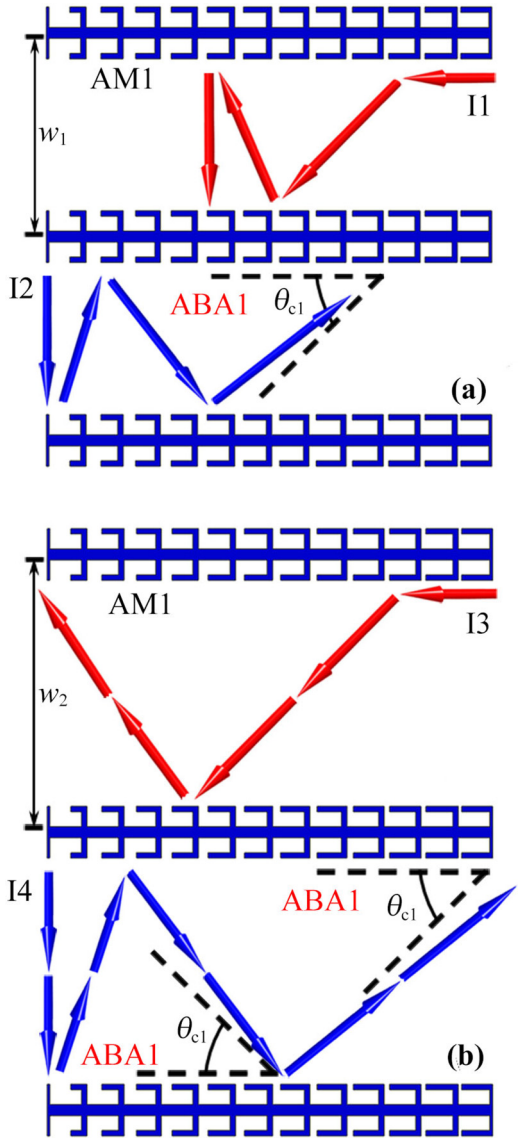

FIG. 5. Schematic of acoustic propagation paths through the open windows with (a) w_1 and (b) w_2 for LI and RI.

and 8.59 rad/m, respectively. The red open circles are the discrete phase delays of six meta-atoms for AM2 and AM3.

Figure 6(b) shows the structures of blades A and B with the composite AM attached on both sides, in which blade B can be obtained by rotating blade A around the red dashed line. Based on blades A and B, we design the second type of open window [shown in Fig. 6(c)], in which the parameter w is fixed and is selected as 10 cm, and the position of blade A can be adjusted along the x direction. By moving blade A with a distance of a, the structure of the open window is displayed in Fig. 6(d). Note that, owing to the symmetry of the open window structure, the simulated results for LI and RI are the same. Thus, we only study the case for LI in the next discussions.

E. Performance of the second type of open windows

Figure 7(a) shows the transmittances of the open window as a function of the parameter a at 3.5 kHz. It is found that

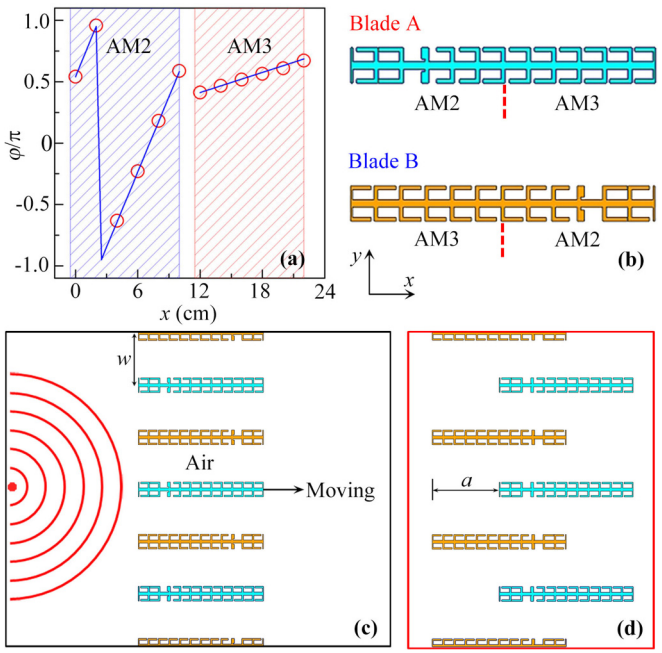

FIG. 6. (a) Theoretical continuous (blue solid line) and discrete (red open circles) phase distribution of the composite AM, which consists of AM2 (blue shadow region) and AM3 (red shadow region). The parameter d of six meta-atoms is 14.1, 16.7, 2.3, 11.0, 12.8, and 14.3 mm for AM2, and 13.6, 13.8, 14.0, 14.2, 14.4, and 14.7 mm for AM3, in which $t = 9.0$ mm for third meta-atom of AM2, and $t = 3.0$ mm for other meta-atoms. (b) Schematic of blades A and B attached with the composite AM on both sides, and the open window (c) before and (d) after moving blade A with a distance of a.

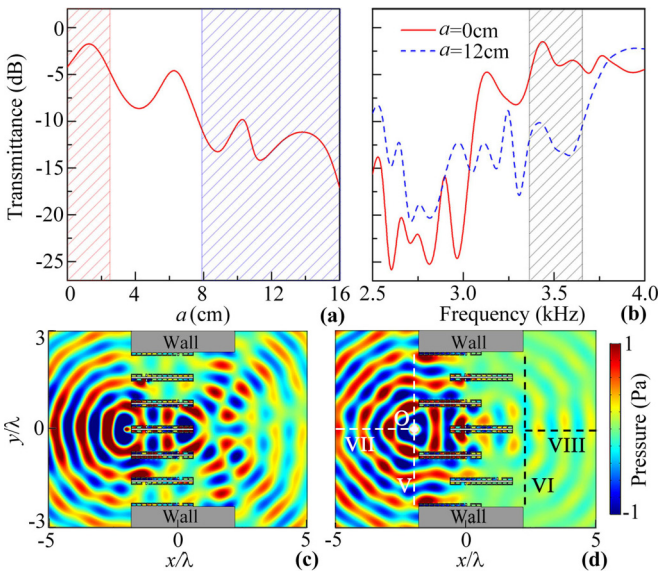

FIG. 7. (a) Simulated transmittances of the second type of open window as a function of the moving distance a. (b) Simulated transmittance spectra of the open window for $a = 0$ and 12.0 cm, and simulated distributions of the pressure field through the open window with (c) $a = 0$ cm and (d) $a = 12.0$ cm at 3.5 kHz. White dot O in (d) represents the position of a cylindrical acoustic source.

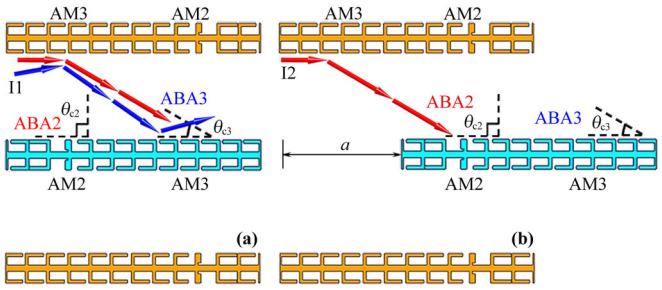

FIG. 8. Schematic of acoustic propagation paths through the open windows with (a) $a = 0$ cm and (b) $a = 12$ cm.

the transmittances are larger than -5 dB with the parameter a below 2.5 cm (red shaded region), indicating that the acoustic wave can transmit through the open window freely. With the increase of a, the transmittances decrease gradually, and are lower than -10 dB in the range 8.0–16.0 cm (blue shaded region). Here, we select $a = 0$ and 12.0 cm to design the open window. Figure 7(b) shows the transmittance spectra of the open window for $a = 0$ and 12.0 cm. In the range 3.4–3.6 kHz (black shaded region), the transmittances are larger than -5 dB for $a = 0$, while those are lower than -10 dB for $a = 12.0$ cm.

Moreover, we simulate the distributions of the pressure field through the open window with $a = 0$ and 12.0 cm at 3.5 kHz. In the case of $a = 0$ [Fig. 7(c)], the transmitted acoustic waves are obvious, which are mainly divided into two symmetric beams about $y = 0$. This is because the reflected paths of the transmitted acoustic wave are manipulated by the same AMs in the upper and lower tunnels of the window, which are symmetric about $y = 0$. However, for $a = 12.0$ cm [Fig. 7(d)], most incident acoustic energy is insulated by the open window, and the transmitted acoustic energy is very weak. Here, we move the cylindrical acoustic source O along the lines V–VIII [shown in Fig. 7(d)], and the corresponding pressure field is shown in the Supplemental Material, Movies V–VIII [44], respectively. The results show that the transmitted acoustic energy is always very weak with different incident positions along the lines V–VIII, which indicates that the acoustic insulation for the second type of open window is also omnidirectional, and can be switched simply by moving the horizontal position of blade A.

F. Mechanism of SOAI for the second type of open windows

To discuss the mechanism of the SOAI of the open window, we display the acoustic propagation paths in the tunnels with $a = 0$ and 12.0 cm [shown in Figs. 8(a) and 8(b)], in which ABA2 and ABA3 correspond to AM2 and AM3, respectively. Based on the phase gradient $d\varphi(x)/dx$ of AM2 and AM3, we calculate the critical angles of AM2 (θ_{c2}) and AM3 (θ_{c3}) as 0° and 60°, and thus the ranges of ABA2 and ABA3 are 0°–90° and 60°–90°, respectively. To simplify the analysis, we select the incident wave with the critical angle of 90°. For $a = 0$ [shown in Fig. 8(a)], the incident wave I1 from the side of blade B (red arrows) in the upper tunnel is first reflected by AM3. Based on Eq. (1), the reflected wave with the angle of 60° impinges into AM3 on blade A, in which this angle is just at the boundary of ABA3. Based on this, when the incident angle of I1 is below 90° (blue arrows), its reflected angle is out the range of ABA3, and therefore the acoustic wave is reflected by AM3 on blade A and transmits through the open window with a positive reflected angle. Here, owing to the structure symmetry, the transmitted wave from the lower tunnel has a negative direction angle. Therefore, the transmitted acoustic pressure field shows two symmetric beams about $y = 0$ [shown in Fig. 7(c)]. But for $a = 12.0$ cm [shown in Fig. 8(b)], AM2 is moved into the original position of AM3. Owing to the larger range of ABA2, the reflected angle of I2 is inevitably in the range of ABA2. Moreover, the incident wave from the side of blade A cannot pass through the open window owing to the existence of ABA2. Therefore, by simply moving the horizontal position of blade A, we realize the second type of the SOAI window without changing the height of the open window.

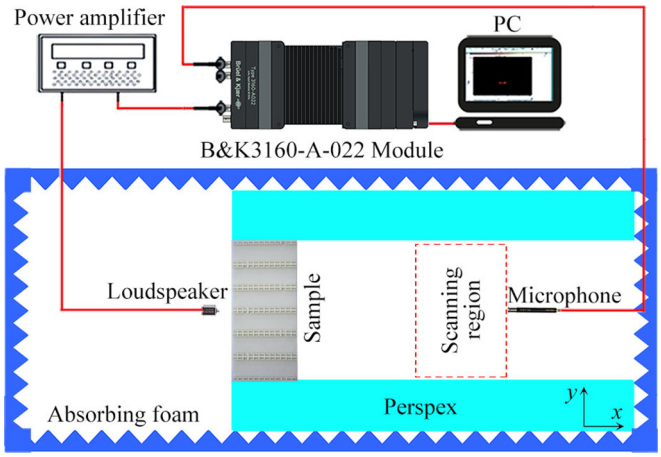

FIG. 9. Experimental setup.

IV. EXPERIMENTAL DEMONSTRATIONS

To experimentally demonstrate the SOAI, we measure the transmittance spectra of the two types of open windows for LI and RI. As shown in Fig. 9, the experimental setup is placed into a planar waveguide composed of two parallel plates (dimension 2 m × 2 m × 1 cm). Wedge-shaped sound-absorbing foams placed at the boundaries of the planar waveguide are used to realize an anechoic environment. To measure transmitted acoustic energy conveniently, the sample is placed in a narrow waveguide which is extended towards the right to cover the scanning region. A balanced armature speaker (Knowles, $7.2 \times 9.5 \times 4.1\,\text{mm}^3$) is adopted as a cylindrical acoustic source, which is located 2.0 cm away from the sample and is driven by a power amplifier. A 0.25-in.-diam microphone (Brüel & Kjær type 4961) is used to detect transmitted acoustic signals in the scanning region. The width of the scanning region in the y direction is the same as that of the waveguide, and the length in the x direction is selected as 15 cm. By using the PULSE LABSHOP software, we can retrieve pressure amplitudes at each position in the scanning region, and the distance between the left side of the scanning region and the sample is 10 cm. The transmittances can be obtained

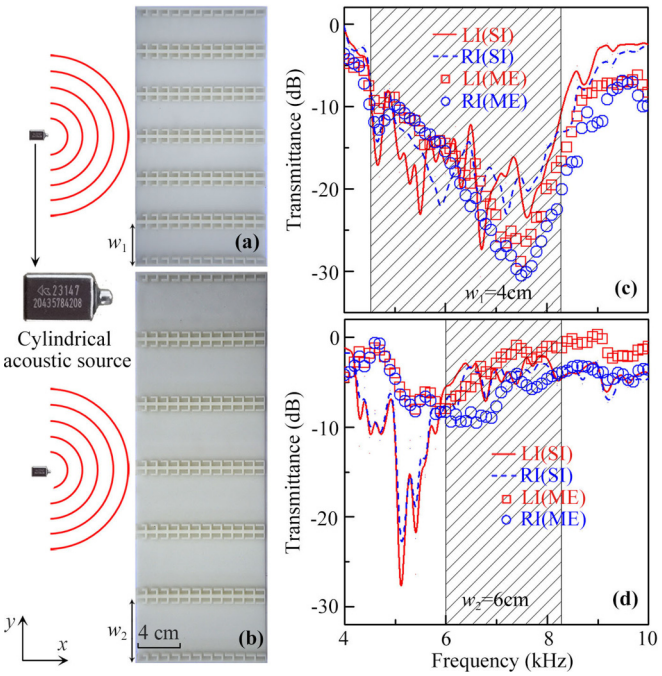

FIG. 10. Photographs of the first type of samples with (a) $w_1 = 4$ cm and (b) $w_2 = 6$ cm. Inset at the left is the photograph of a cylindrical acoustic source. Simulated (SI) and measured (ME) transmittance spectra of the samples with (c) $w_1 = 4.0$ cm and (d) $w_2 = 6.0$ cm for LI and RI.

by using $T = \frac{\int A_1^2 ds}{\int A_2^2 ds}$, in which A_1 and A_2 are the measured pressure amplitudes at each position in the scanning region with and without the sample, respectively.

Figures 10(a) and 10(b) show the photographs of the first type of samples, in which the sizes of both samples are half of those in Figs. 4(a) and 4(b) owing to the size limitation of our experiment platform. Figures 10(c) and 10(d) show the simulated and measured transmittance spectra for both samples. It is found that, in the working bands [shaded region, twice that in Figs. 4(a) and 4(b)], the measured results show the high SOAI effect and agree well with the simulated ones. However, there also exists a large difference between measured and simulated results below 5.8 kHz, especially in Fig. 10(d), which is attributed to the undesired scattering and imperfect absorption of acoustic waves at the low-frequency range.

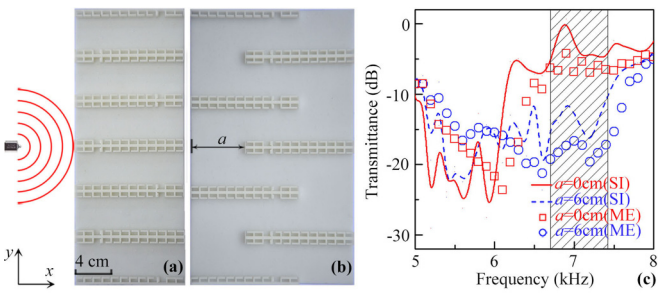

FIG. 11. Photographs of the second type of samples with (a) $a = 0$ cm and (b) $a = 6$ cm. (c) Simulated and measured transmittance spectra of the samples with $a = 0$ and 6.0 cm.

As shown in Figs. 11(a) and 11(b), the second type of the samples with $a = 0$ and 6.0 cm are also reduced by twice that in Figs. 6(c) and 6(d). It is found that the measured transmittance spectra also show a typical SOAI phenomenon [shown in Fig. 11(c)], and agree well with the simulated results. The aforementioned results experimentally demonstrate the feasibility of the two types of open window structures.

V. CONCLUSION

In conclusion, we have demonstrated two types of open window structures with the SOAI effect numerically and experimentally. Both types of open window structures are composed of an array of blades that are attached with ultrathin AMs on both sides. The omnidirectional sound insulation effect in both cases arises from the acoustic manipulation ability of the ultrathin AMs. Our results show that, in the first type, the fractional bandwidth of the omnidirectional insulation can reach about 0.58 with $w = 8$ cm. By increasing the distance w to 10.3 cm, the acoustic waves can transmit through the open window. The second type of open window is composed of an alternative arrangement of two types of blades, in which the SOAI effect can be obtained by horizontally moving one kind of blade. The measured results agree well the simulated ones. The proposed two types of open windows show the unusual features of broadband omnidirectional acoustic insulation with switchable functionality, which may have great potential in a variety of practical applications, such as noise control, mechanical engineering, and architectural acoustics.

ACKNOWLEDGMENTS

This work was supported by the National Natural Science Foundation of China (Grants No. 11774137, No. 51779107, No. 61671314, and No. 11634005), the National Key R&D Program of China (Grant No. 2017YFA0303702), the Six Talent Peaks Project in Jiangsu Province (Grant No. GDZB-019), the China Postdoctoral Science Foundation (Grant No. 2017M621643), and the Natural Science Foundation of Jiangsu Higher Education Institutions of China (Grant No. 18KJB140003), and the Jiangsu Qing Lan Project.

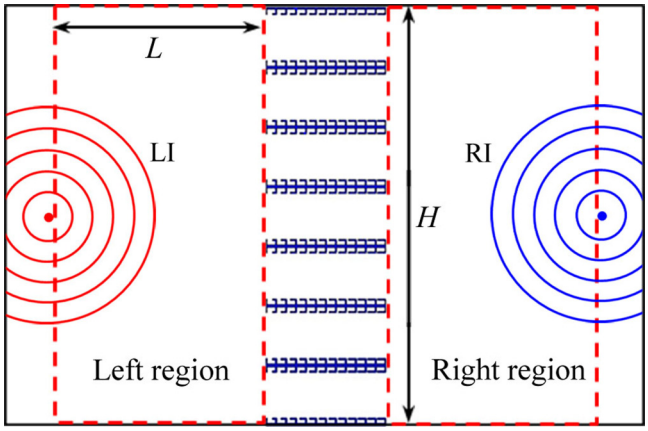

FIG. 12. Schematic of transmitted and reflected intensity calculation method.

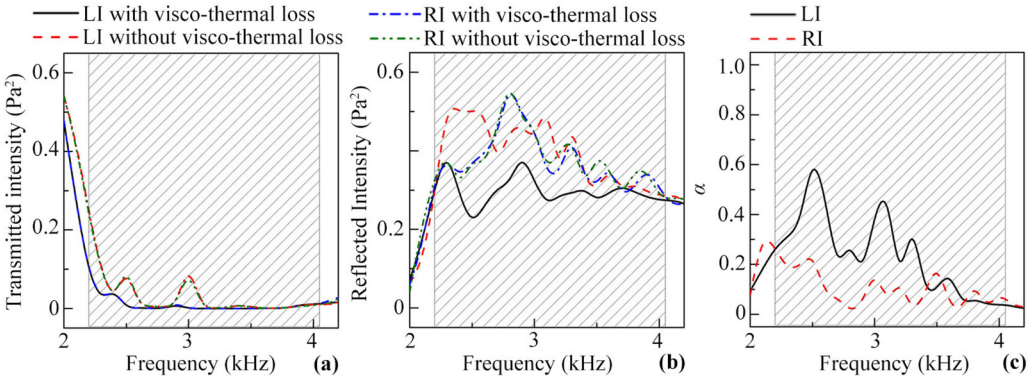

FIG. 13. (a) Transmitted and (b) reflected intensity spectra induced by the open window with and without the viscothermal loss, and (c) absorption coefficients of the open window with the viscothermal loss. The distance w between two adjacent blades is 8 cm.

APPENDIX: INFLUENCES OF THE VISCOTHERMAL LOSS ON THE OMNIDIRECTIONAL ACOUSTIC INSULATION OF THE OPEN WINDOW

To investigate the influences of the viscothermal loss on the omnidirectional acoustic insulation, we simulate the transmitted and reflected intensities induced by the first type of open window with and without the viscothermal loss. As shown in Fig. 12, two red dashed rectangles with the same size at the left and right sides of the open window are set as integration regions, in which the length L is 15 cm, and the height H is the same as that of the window. The cylindrical acoustic source is placed at a distance of 15.5 cm away from the window for LI and RI. To obtain the reflected intensity, the background pressure field for the cylindrical wave is adopted in the left (right) region for LI (RI), and the reflected intensity can be obtained by integrating acoustic intensity in the left (right) region for LI (RI), while the transmitted intensity is calculated by integrating acoustic intensity in the right (left) region for LI (RI).

Figures 13(a) and 13(b) show the transmitted and reflected intensity spectra induced by the open window with and without the viscothermal loss for LI and RI, respectively. It is found that, by introducing the viscothermal loss, the transmitted intensity is lower than that without viscothermal loss below 3.5 kHz for LI and RI [Fig. 13(a)]. Therefore, by introducing the viscothermal loss, the transmitted acoustic energy becomes much weaker in the working band (black shaded region), and the performance of the omnidirectional sound insulation is improved owing to sound energy loss. Moreover, as shown in Fig. 13(b), for LI, the reflected intensity with the viscothermal loss (black solid line) is much smaller than that without the viscothermal loss (red dashed line). But for RI, the difference between the reflected intensities with and without viscothermal loss is relatively small. This is because the sound insulation for LI arises from the ABA [shown in Fig. 5(a)], and thus the reflected acoustic energy propagates along the AM [shown in Fig. 2(b)], leading to much stronger loss of sound energy inside the hooklike meta-atoms. However, the sound insulation for RI is attributed to multiple reflections between the upper and lower AMs [shown in Fig. 5(a)], and therefore the energy loss is relatively weak. Figure 13(c) shows the absorption coefficients (α) of the open window with the viscothermal loss for LI and RI. It is found that, in the working band, the absorption coefficient for LI is much larger than that for RI. The aforementioned results indicate that, by introducing the viscothermal loss in the open window, the performance of the omnidirectional sound insulation is improved owing to sound energy loss, and the absorption coefficient for LI is much larger than that for RI.

[1] Z. Y. Liu, X. X. Zhang, Y. W. Mao, Y. Y. Zhu, Z. Y. Yang, C. T. Chan, and P. Sheng, Locally resonant sonic materials, Science **289**, 1734 (2000).

[2] N. Fang, D. Xi, J. Xu, M. Ambati, W. Srituravanich, C. Sun, and X. Zhang, Ultrasonic metamaterials with negative modulus, Nat. Mater. **5**, 452 (2006).

[3] M. H. Lu, C. Zhang, L. Feng, J. Zhao, Y. F. Chen, Y. W. Mao, J. Zi, Y. Y. Zhu, D. N. Zhu, and N. B. Ming, Negative birefraction of acoustic waves in a sonic crystal, Nat. Mater. **6**, 744 (2007).

[4] J. Li, L. Fok, X. B. Yin, G. Bartal, and X. Zhang, Experimental demonstration of an acoustic magnifying hyperlens, Nat. Mater. **8**, 931 (2009).

[5] J. Christensen and F. J. deAbajo, Anisotropic Metamaterials for Full Control of Acoustic Waves, Phys. Rev. Lett. **108**, 124301 (2012).

[6] Y. Lai, Y. Wu, P. Sheng, and Z. Q. Zhang, Hybrid elastic solids, Nat. Mater. **10**, 620 (2011).

[7] Z. Liang and J. Li, Extreme Acoustic Metamaterial by Coiling Up Space, Phys. Rev. Lett. **108**, 114301 (2012).

[8] S. A. Cummer, J. Christensen, and A. Alù, Controlling sound with acoustic metamaterials, Nat. Rev. Mater. **1**, 16001 (2016).

[9] Y. Li, B. Liang, Z. M. Gu, X. Y. Zou, and J. C. Cheng, Reflected wavefront manipulation based on ultrathin planar acoustic metasurfaces, Sci. Rep. **3**, 2546 (2013).

[10] K. Tang, C. Y. Qiu, M. Z. Ke, J. Y. Lu, Y. T. Ye, and Z. Y. Liu, Anomalous refraction of airborne sound through ultrathin metasurfaces, Sci. Rep. **4**, 6517 (2014).

[11] Y. B. Xie, W. Q. Wang, H. Y. Chen, A. Konneker, B.-I. Popa, and S. A. Cummer, Wavefront modulation and subwavelength diffractive acoustics with an acoustic metasurface, Nat. Commun. **5**, 5553 (2014).

[12] G. C. Ma, M. Yang, S. W. Xiao, Z. Y. Yang, and P. Sheng, Acoustic metasurface with hybrid resonances, Nat. Mater. **13**, 873 (2014).

[13] B. Y. Xie, K. Tang, H. Cheng, Z. Y. Liu, S. Q. Chen, and J. G. Tian, Metasurfaces: Coding acoustic metasurfaces, Adv. Mater. **29**, 1603507 (2017).

[14] Y. Li, C. Shen, Y. B. Xie, J. F. Li, W. Q. Wang, S. A. Cummer, and Y. Jing, Tunable Asymmetric Transmission via Lossy Acoustic Metasurfaces, Phys. Rev. Lett. **119**, 035501 (2017).

[15] M. Yang, G. Ma, Z. Yang, and P. Sheng, Coupled Membranes with Doubly Negative Mass Density and Bulk Modulus, Phys. Rev. Lett. **110**, 134301 (2013).

[16] X. Wang, H. Zhao, X. Luo, and Z. Huang, Membrane-constrained acoustic metamaterials for low frequency sound insulation, Appl. Phys. Lett. **108**, 041905 (2016).

[17] T. Y. Huang, C. Shen, and Y. Jing, On the evaluation of effective density for plate- and membrane-type acoustic metamaterials without mass attached, J. Acoust. Soc. Am. **139**, 3240 (2016).

[18] L. Y. L. Ang, Y. K. Koh, and H. P. Lee, Broadband sound transmission loss of a large-scale membrane-type acoustic metamaterial for low-frequency noise control, Appl. Phys. Lett. **111**, 041903 (2017).

[19] J. Mei, G. Ma, M. Yang, Z. Yang, W. Wen, and P. Sheng, Dark acoustic metamaterials as super absorbers for low-frequency sound, Nat. Commun. **3**, 756 (2012).

[20] J. Li, W. Wang, Y. Xie, B. I. Popa, and S. A. Cummer, A sound absorbing metasurface with coupled resonators, Appl. Phys. Lett. **109**, 091908 (2016).

[21] V. Romero-García, G. Theocharis, O. Richoux, A. Merkel, V. Tournat, and V. Pagneux, Perfect and broadband acoustic absorption by critically coupled sub-wavelength resonators, Sci. Rep. **6**, 19519 (2016).

[22] H. Long, Y. Cheng, and X. J. Liu, Asymmetric absorber with multiband and broadband for low-frequency sound, Appl. Phys. Lett. **111**, 143502 (2017).

[23] V. Leroy, A. Strybulevych, M. Lanoy, F. Lemoult, A. Tourin, and J. H. Page, Superabsorption of acoustic waves with bubble metascreens, Phys. Rev. B **91**, 020301 (2015).

[24] N. Sui, X. Yan, T.-Y. Huang, J. Xu, F.-G. Yuan, and Y. Jing, A lightweight yet sound-proof honeycomb acoustic metamaterial, Appl. Phys. Lett. **106**, 171905 (2015).

[25] W. W. Yu, L. Fan, R. H. Ma, H. Zhang, and S. Y. Zhang, Low-frequency and multiple-bands sound insulation using hollow boxes with membrane-type faces, Appl. Phys. Lett. **112**, 183506 (2018).

[26] C. Gaulon, J. Pierre, C. Derec, L. Jaouen, F. X. Becot, F. Chevillotte, F. Elias, W. Drenckhan, and V. Leroy, Acoustic absorption of solid foams with thin membranes, Appl. Phys. Lett. **112**, 261904 (2018).

[27] H. Long, S. X. Gao, Y. Cheng, and X. J. Liu, Multiband quasi-perfect low-frequency sound absorber based on double-channel Mie resonator, Appl. Phys. Lett. **112**, 033507 (2018).

[28] X. Cai, Q. Guo, G. Hu, and J. Yang, Ultrathin low-frequency sound absorbing panels based on coplanar spiral tubes or coplanar Helmholtz resonators, Appl. Phys. Lett. **105**, 121901 (2014).

[29] Y. Li and B. M. Assouar, Acoustic metasurface-based perfect absorber with deep subwavelength thickness, Appl. Phys. Lett. **108**, 063502 (2016).

[30] C. Zhang and X. Hu, Three-Dimensional Single-Port Labyrinthine Acoustic Metamaterial: Perfect Absorption with Large Bandwidth and Tunability, Phys. Rev. Appl. **6**, 064025 (2016).

[31] L. Liu, H. Chang, C. Zhang, and X. Hu, Single-channel labyrinthine metasurfaces as perfect sound absorbers with tunable bandwidth, Appl. Phys. Lett. **111**, 083503 (2017).

[32] C. Shen and S. A. Cummer, Harnessing Multiple Internal Reflections to Design Highly Absorptive Acoustic Metasurfaces, Phys. Rev. Appl. **9**, 054009 (2018).

[33] P. Wei, C. Croënne, S. T. Chu, and J. Li, Symmetrical and anti-symmetrical coherent perfect absorption for acoustic waves, Appl. Phys. Lett. **104**, 121902 (2014).

[34] J. Z. Song, P. Bai, Z. H. Hang, and Y. Lai, Acoustic coherent perfect absorbers, New J. Phys. **16**, 033026 (2014).

[35] C. Meng, X. Zhang, S. T. Tang, M. Yang, and Z. Yang, Acoustic coherent perfect absorbers as sensitive null detectors, Sci. Rep. **7**, 43574 (2017).

[36] Y. Cheng, C. Zhou, B. G. Yuan, D. J. Wu, Q. Wei, and X. J. Liu, Ultra-sparse metasurface for high reflection of low-frequency sound based on artificial Mie resonances, Nat. Mater. **14**, 1013 (2015).

[37] C. Shen, Y. Xie, J. Li, S. A. Cummer, and Y. Jing, Acoustic metacages for sound shielding with steady air flow, J. Appl. Phys. **123**, 124501 (2018).

[38] R. Ghaffarivardavagh, J. Nikolajczyk, S. Anderson, and X. Zhang, Ultra-open acoustic metamaterial silencer based on Fano-like interference, Phys. Rev. B **99**, 024302 (2019).

[39] Y. F. Zhu, Z. M. Gu, B. Liang, J. Yang, J. Yang, L. L. Yin, and J. C. Cheng, Asymmetric sound transmission in a passive non-blocking structure with multiple ports, Appl. Phys. Lett. **109**, 103504 (2016).

[40] Y. Ge, H. X. Sun, S. Q. Yuan, and J. P. Xia, Asymmetric acoustic transmission in an open channel based on multiple scattering mechanism, Appl. Phys. A **123**, 328 (2017).

[41] H. L. Zhang, Y. F. Zhu, B. Liang, J. Yang, J. Yang, and J. C. Cheng, Omnidirectional ventilated acoustic barrier, Appl. Phys. Lett. **111**, 203502 (2017).

[42] Y. Ge, H. X. Sun, S. Q Yuan, and Y. Lai, Broadband unidirectional and omnidirectional bidirectional acoustic insulation through an open window structure with a metasurface of ultrathin hooklike meta-atoms, Appl. Phys. Lett. **112**, 243502 (2018).

[43] N. F. Yu, P. Genevet, M. A. Kats, F. Aieta, J. P. Tetienne, F. Capasso, and Z. Gaburro, Light propagation with phase discontinuities: Generalized laws of reflection and refraction, Science **334**, 333 (2011).

[44] See Supplemental Material at http://link.aps.org/supplemental/10.1103/PhysRevMaterials.3.065203 for the transmittance simulation method, the transmittance spectra of the first type of open window with $w = 15$ cm, and the design of the open window with SOAI around 1.0 kHz based on improved hooklike meta-atoms. Supplemental Movies show the omnidirectional acoustic insulation for the first type of open window (Movies I–IV) and for the second type of open window (Movies V–VIII).